Vacuum 243 (2026) 114784

Contents lists available at ScienceDirect

Vacuum

journal homepage: www.elsevier.com/locate/vacuum

Evaluation of a novel PECVD reactor for the intended continuous coating of flexible web material

Philipp Alizadeh *, Rainer Dahlmann

Institute for Plastics Processing (IKV) in Industry and Craft at RWTH Aachen University, 52074, Aachen, Germany

ARTICLE INFO

Handling editor: Prof. L.G. Hultman

Keywords:
PECVD
Reactor development
Gas barrier coating
Inline vacuum processing

ABSTRACT

PET film samples were coated on a novel Plasma-Enhanced Chemical Vapor Deposition (PECVD) reactor. The reactor represents a pioneering development as the first of its kind to be designed for the continuous coating of plastic film. The reactor is equipped with sequentially arranged airlocks, that facilitate a gradual reduction in pressure from ambient pressure to process pressure levels of a few pascals. The airlocks are equipped with slits that facilitate the uninterrupted introduction and extraction of the web material. In the experiments presented however, the film was positioned manually in the reactor to eliminate any potential influence from sliding contacts or similar mechanical stresses associated with film transport. The leakage flows associated with the airlocks were present in a manner consistent with subsequent automated operation. An investigation of the leakages was published earlier.

In the study presented here, the utilization of OTR measurements was instrumental in demonstrating the potential to align the coating process with the airlock system. Depending on the position inside the coating area, barrier against oxygen was improved by factors of up to 29. Furthermore, coating thickness measurements were utilized to show that the coating of the reactor walls was significantly reduced by using a process envelope.

1. Introduction

Plastic packaging combines high demands on product protection and cost-effectiveness like hardly any other material. They can be produced and processed extremely cost-effectively, but this advantage has meant that recycling is often less economical than producing new goods. Only 48.7 % of municipal waste in the European Union was recycled after use in 2022. Packaging accounts for around 36 % of municipal waste, making it a significant proportion of the total waste generated [1].

The resulting burden on our ecosystems due to non-recycled waste has been recognized and measures to protect them, such as the EU Waste Directive 2008/98/EC, have been enacted [2].

Sustainability requirements pose new challenges for packaging manufacturers. Product protection to reduce food waste can often only be achieved with conventional plastic packaging by limiting its recyclability. Multilayer composites, which meet the various requirements using a combination of different materials, are often no longer economically separable after use, meaning that they cannot be recycled.

Plasma-enhanced chemical vapor deposition (PECVD) is one of the few processes capable of meeting all of the requirements described. PECVD technology has rapidly established itself in the hollow container sector in recent years. Today, PET beverage bottles can be coated with a throughput of several 10,000 bottles per hour [3]. The concept for hollow body internal coating was developed by Plein and patented in 1986 [4]. In the field of flexible packaging, the use of PECVD technology is much less widespread. The reasons for this can be explained by using the concept for the internal coating of hollow bodies.

The system concept provides for the positioning of a hollow body in the reactor. The hollow body is evacuated simultaneously with the vacuum chamber. Process gases are fed into the interior of the hollow body creating a stationary gas flow. Finally, microwave radiation is fed into the reactor. The key feature is that the substrate contains the process gas inside, which is excited to form a plasma. The configuration is therefore referred to below as “in-plasma”. It has several key properties that have resulted in the configuration being used in this way or in a modified form in a large number of industrial systems and patents [5–7]. The most important properties include a high coating deposition rate, a comparatively low degree of parasitic coatings and a high volume yield.

The process is designed in such a way that a pressure difference is created between the inside of the hollow body and the ambient volume.

* Corresponding author. IKV, 502047, Aachen, Germany.
E-mail address: publications@ikv.rwth-aachen.de (P. Alizadeh).

https://doi.org/10.1016/j.vacuum.2025.114784
Received 19 July 2025; Received in revised form 14 September 2025; Accepted 28 September 2025
Available online 29 September 2025
0042-207X/© 2025 The Authors. Published by Elsevier Ltd. This is an open access article under the CC BY-NC-ND license (http://creativecommons.org/licenses/by-nc-nd/4.0/).

According to the ignition conditions for microwave plasmas, analogous to Paschen's law, this results in preferred ignition conditions within the hollow body [8,9].

When comparing coating processes for flexible substrates with hollow body coating, two key aspects can be identified with regard to the feasible economic efficiency. Firstly, an adaptation of the in-plasma principle is challenging due to the idealized two-dimensional film geometry and secondly, discontinuous processes mean a significant intervention in the continuous film production process. In contrast to films, bottles are always processed discontinuously. Classic process steps include the injection molding of pre-forms, stretch blow molding to produce the bottle geometry, filling, labeling, etc.

Films, on the other hand, are processed completely continuously wherever possible. Each discontinuous processing step means a costly intervention in the automated process chain. As a result, flexible packaging can often be produced more economically using continuous conventional processes (multi-material composites). Although there is great demand for PVD and PECVD processes in the field of flexible food packaging, high system costs are seen as a decisive obstacle to wider adaptation of the technology [10–12]. With increasingly strict regulatory framework conditions, the need for action to adapt flexible, recyclable packaging solutions is growing [13]. It can therefore be assumed that the need for economical processes for the functionalization of flexible substrates will increase significantly [14].

Based on this demand, a new type of reactor was developed for the low-maintenance, continuous coating of flexible plastic substrates using the in-plasma principle. The reactor has an airlock system that enables sequential pressure reduction, with slits provided for film transport. Furthermore, the reactor has a process envelope that spatially confines the plasma analogous to the inner bottle coating.

The vacuum technical investigation, which poses the first milestone in validating the reactor concept, has been published earlier [15]. As part of this investigation, the reactor prototype used here was examined with regard to its pressure state. The focus was on leakage flows at the airlocks and at the process envelope. Furthermore, the influence of oxygen feed into the process shell on the pressure distribution in the reactor was already investigated. The necessary pressure difference between the process envelope and the environment as well as the necessary general pressure level, taking into account the leakages occurring, were evaluated positively. All results shown here were obtained using the same reactor setup.

The results presented here are based on the first coating experiments in this reactor, which pose the second milestone in validating the reactor concept. The aim of the study presented here is to evaluate the feasibility of combining the in-plasma configuration with a leakage-afflicted airlock system. The samples were positioned in the reactor manually to rule out any possible damaging from the film transport. The automatic feeding of the film is planned for the future as the third and final milestone in validating the reactor concept.

It should be noted that the barrier values achieved do not represent the technically possible limit of the system technology but serve to assess the basic feasibility of the system concept. To this end, a two-layer coating was first developed that has a significant barrier effect against oxygen. The spatial dependence of the layer deposition rates as well as the barrier effect was investigated for this coating system. Furthermore, the individual layers were characterized using FT-IR to enable categorization in the spectrum of SiOCH and SiO_x coatings. In addition, layer deposition rates on the chamber walls and outlets of the process envelope were investigated in order to be able to assess the cleaning effort during operation of the system.

2. Materials and methods

A 3D-model of the coating reactor is displayed in Fig. 1. The reactor has three airlocks, which serve to ensure a gradual reduction in pressure. The airlocks have slits (vertical in Fig. 1) with a length (l) of 90 mm, a width (w) of 402 mm and a height (h) of 0.1 mm that allow the film to be transported in and out of the reactor. Consequently, a leakage flow into the chamber is tolerated in order to prevent any damage to the coating by means of touching components. The film is to be transported using a drive inside the reactor and another drive and brake outside the reactor. The film is first fed into the reactor via one of the two slits and runs through it to the cooling roller at the end of the reactor. There, the film is deflected by 180° and passes through the entire reactor again to the second slit of the first airlock module.

Due to the airlocks, there are four pressure zones in the reactor, which have separate pumping units. In the coating chamber (Fig. 2) there is also a process envelope that spatially confines the plasma analogue to the internal bottle coating. The envelope also has corresponding slits to ensure a pressure gradient between the process envelope and the surrounding chamber volume and at the same time to enable the film to be fed in and out. The turbo molecular pump (TMP) is connected to the surrounding volume of the coating chamber with a view to reducing the pressure relative to the process envelope and thereby containing plasma excitation to the inner volume of the envelope. The process envelope is equipped with two pipes for process gas

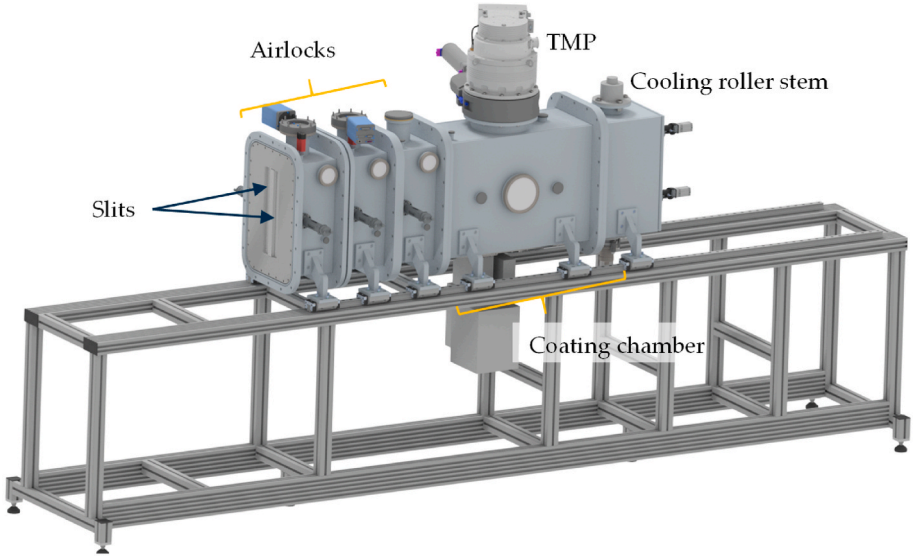

Fig. 1. 3D-model of the coating reactor for continuous coating of flexible webs.

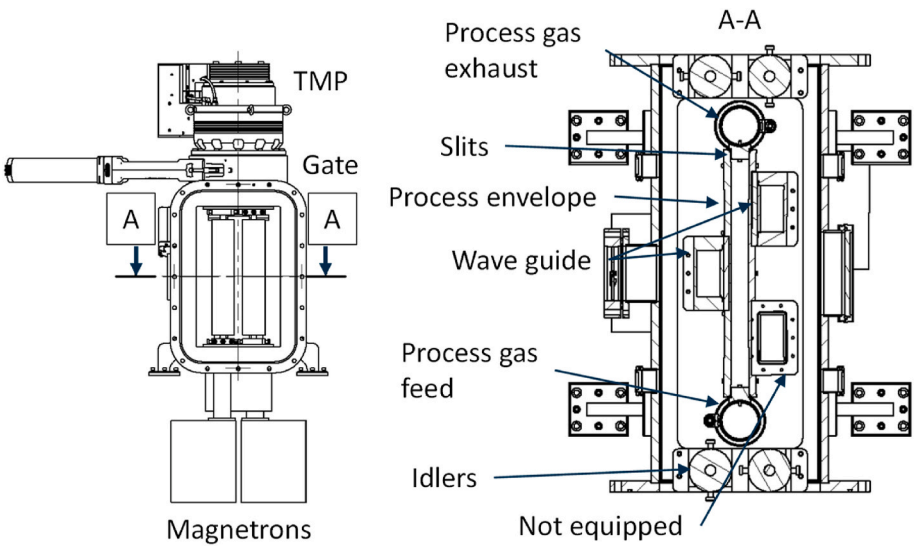

Fig. 2. Side view (left) and sectional top view (right) of the coating chamber.

supply and extraction, each with 12 holes with a diameter of 10 mm. Microwave radiation is fed in over the entire height of the process envelope using two vertically installed waveguides with a width of 470 mm. The waveguides are positioned at the vertical line of symmetry (Fig. 2 right - center rectangular duct) and 118 mm off center (Fig. 2 right - upper rectangular duct). The third waveguide flange (Fig. 2 right - lower rectangular duct) is not in use and closed with a blind flange.

In the context of the work presented here, however, the focus is on the coating process. As the results presented here are the first coating experiments in the reactor, the film was not fed through continuously, but samples were replaced manually in order to initially rule out damaging the coatings as a result of the film feed. However, all tests were carried out with open airlocks, so that the same vacuum conditions prevailed as in a continuous low-pressure coating process.

The coating deposition was carried out on a film substrate made of biaxially orientated polyethylene terephthalate (BO-PET, thickness 12 µm, Flex Films Inc.). The monomer used was hexamehyldisiloxane (HMDSO) with a purity of 98.5 % from Merck KGaA, Germany. The oxygen gas used for the synthesis and permeation measurements and the nitrogen used as carrier gas for the permeation measurements had a purity of at least 99.999 % (both gases were supplied by Westfalen AG, Germany).

Polished Si wafers from Si-Mat – Silicon Materials e.K., Germany were used to deter-mine the layer thicknesses. The layer thickness was measured using tactile profilometry with an Alpha-Step® D-600 Stylus Profiler from KLA-Tencor GmbH, Germany. Five measurements were averaged in each case, unless otherwise specified. The measuring distance was 2 mm for all measurements. The measuring speed was 0.1 mm/s. The con-tact force was set according to the hardness of the substrates within a range of 2 mg–0.5 mg force equivalents (device-specific unit).

An M8001 from Systech Instruments Ltd., UK was used to determine the oxygen transmission rates (OTR) of the analyzed BO PET film substrates and the deposited coatings. Dry oxygen was used as the test gas and dry nitrogen as the carrier gas. The measurement temperature was kept at 23 °C.

The FTIR spectra were performed using a Bruker Equinox 55 spectrometer from Bruker Corporation, USA, in attenuated total reflectance (ATR) mode with a diamond crystal and potassium bromide beamsplitter. The spectra were recorded in the range between 680 and 4000 cm-1 with a resolution of ≈1 cm-1. Depending on the sample, the wavelength-dependent analysis depth can be several micrometers. The method is therefore only suitable to a limited extent for analyzing nanoscale plasma polymers on plastics. Gold-coated silicon wafers were therefore used as the substrate for the analyses. Gold is not IR-active, so that any influence on the measurements by the underlying substrate is minimized. At least three spectra were averaged for each measurement. The wave number distribution and corresponding functional groups on which the FTIR analysis is based can be found in Table 1.

The utilized coating parameters are displayed in Table 2.

The process parameters consist of the mass flow rates of HMDSO and oxygen as process gases, the microwave parameters, the coating time and the process pressure. The micro wave power is introduced in a pulsed mode. The parameter referenced to as power equals to the amplitude power during the “Pulse on” time. During “Pulse off” time no power is introduced into the process. The process can be fully controlled using the seven setting parameters shown above. The layer properties can be set over a wide range of functionalities using the seven setting parameters.

The coating system shown in Table 2 has two layers. It was shown in earlier studies, that to improve the growth behavior of the barrier layer (SiO_x) an organic intermediate layer (SiOCH) can be beneficial. The intermediate layer, whose chemical structure is organic, promotes adhesion between the substrate and the barrier layer. It is also able to compensate for rough surface topologies and protect sensitive substrates from degradation due to aggressive oxygen ions during the application of the barrier layer. The organic functional groups are able to form covalent bonds with both the substrate and the inorganic barrier layer.

A process gas ratio (precursor/auxiliary gas) of approx. 2 % was used for the application of the barrier layer. The particularly high oxygen content prevents volume polymerization and promotes the formation of an inorganic layer network through the implantation of atomic oxygen and the replacement of carbon from the monomer [17]. The process

Table 1
Association of wave numbers with vibration modes of selected functional groups [16].

Vibration Mode	Wave number [cm^{-1}]
b Si-O-Si, s Si-C, r CH_3	800
r Si-CH_3, b Si$(CH_3)_3$	839
s_{sym} Si-OH	930
s_{anti} Si-O-Si network	1070
s_{anti} Si-O-Si cage	1135
s_{sym} CH_3 in Si-$(CH_3)_x$	1257

Prefixes: s = stretching; b = bending; r = rocking.
Subscript: anti = anti symmetrical; sym = symmetrical.

Table 2
Parameters for the application of a barrier coating system in the developed reactor for film substrates.

Name	Process gas		Micro wave power			Process time	Process pressure
	Precursor	Auxiliary gas	Power	Pulse on	Pulse off	t_B [s]	p [Pa]
	HMDSO [sccm]	O_2 [sccm]	P [W]	t_{on} [ms]	t_{off} [ms]		
Intermediate layer (SiOCH)	125	0	800	2	100	8	8
Barrier layer (SiO_x)	20	1000	2500	6	100	35	23

chamber pressure (surrounding the process envelope) was kept below 2 Pa for all experiments in order to mitigate ignition of a plasma outside the envelope.

Figs. 3 and 4 show vertical sectional views through the coating chamber. The dimensions (l x w x h) of the process envelope are approx. 424 mm × 404 mm x approx. 32.7 mm (average wall distance). The resulting volume is approx. 5.6 L. Samples are taken from the film webs fixed in the process envelope after coating, the position of which is shown in Figs. 3 and 4. Samples are taken in a spatially resolved manner to be able to conduct a spatially resolved analysis of the coating. Both the variation with regard to the film width (vertical) and the positional dependence with regard to the intended conveying direction (horizontal) are decisive. The vertical homogeneity is decisive for the complete functionalization of the film with regard to its width. Based on the horizontal homogeneity, statements can be made about the layer deposition depending on the position relative to the waveguides and the process gas supply and extraction.

The films were attached to both sides of the process envelope for coating. From the system operator's perspective, the front side of the process sleeve is intended for the incoming film (left wall of the process envelope in Fig. 2). The labelling is done accordingly (e.g. front, left, center - FLC). For the film thickness measurements, polished silicon wafers were attached at the same positions where the film was removed.

The waveguides are arranged in the center of the front wall and on the left-hand side of the rear wall. Depending on the arrangement of the waveguides, one of the vertical rows is located directly on a waveguide or directly opposite a waveguide. According to the nomenclature, the process gases are introduced from the right and extracted on the left, so that the rows on the left are located in the downstream area of the center row.

In the area of the gas inlet (right), which is not equipped with a waveguide, no samples were taken into account. This is due to the fact that no layer deposition could be observed in this area during preliminary investigations. Consequently, the volume of the first third of the process envelope can be ignored when considering the molecule retention time.

3. Results and discussion

In this section, an evaluation of the system concept is conducted on the basis of the properties of the deposited coatings. To this end, analyses of the layer thickness distribution within the process envelope and parasitic coatings on the chamber walls, the chemical composition and the barrier effect against oxygen are presented.

3.1. Coating thickness distribution within the process envelope

As the plasma properties vary greatly depending on the process parameters, a layer thickness distribution within the process envelope was initially determined separately for both layers (Table 2). The results can be found in Tables 3 and 4.

As the evaluation of the coating thickness for SiOCH coatings is made more difficult by their soft structure, the coating thickness distribution was determined for a coating time of 80 s in contrast to Table 2. As the resolution of the measuring system does not allow any reliable conclusions to be drawn for coating thicknesses below 5 nm, the measurements concerned were labelled accordingly.

It is noticeable that the SiOCH layer only has high layer thicknesses on the wafers that are positioned directly in front of the waveguides. Deposition rates vary highly depending on position from values of 0,1 nm/s to 0,5 nm/s. Consequently, the plasma does not penetrate the volume of the process envelope deep enough to coat the opposite wall. This could be related to the higher process pressure during the deposition of the SiOCH layer, as this reduces the mean free path of the particles [18]. While the wafers on the center waveguide show greater variation, the wafers on the left waveguide appear to be much more

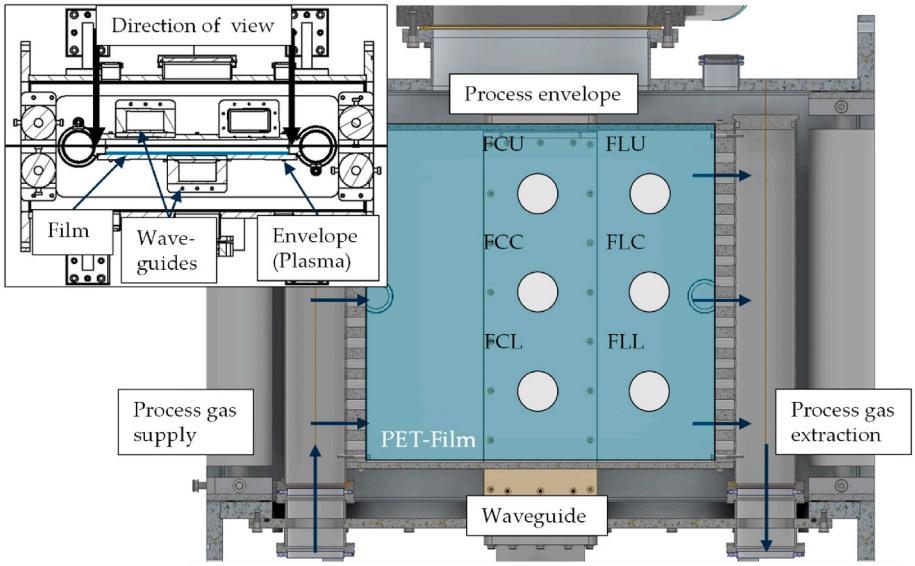

Fig. 3. Sectional view of the front half of the coating chamber.

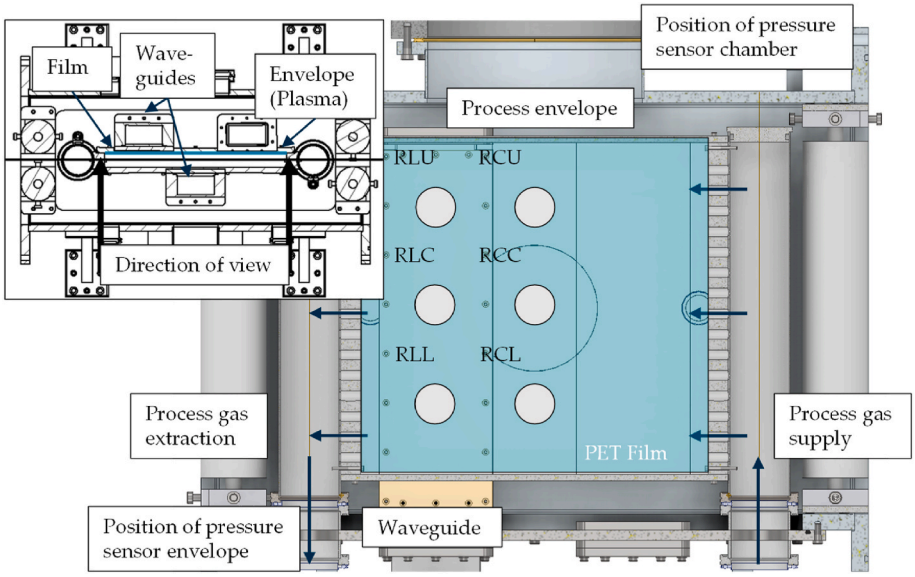

Fig. 4. Sectional view of the rear half of the coating chamber.

Table 3
Layer thickness distribution for the SiOCH layer after 80 s of coating time.

Position	Left-hand side (L)	Center (C)
Coating thicknesses [nm] for the front wall of the process envelope		
Upper (U)	7,6 ± 1.9 (FLU)	20.4 ± 3.8 (FCU)
Center (C)	<5 (FLC)	38.0 ± 2.1 (FCC)
Lower (L)	<5 (FLL)	7.8 ± 2.1 (FCL)
Coating thicknesses [nm] for the rear wall of the process envelope		
Upper (U)	28.2 ± 3.5 (RLU)	<5 (RCU)
Center (C)	28.2 ± 3.0 (RLC)	<5 (RCC)
Lower (L)	30.6 ± 4.3 (RLL)	<5 (RCL)

Table 4
Coating thickness distribution for the SiOx coating according to Table 2.

Position	Left-hand side	Center
Coating thicknesses [nm] for the front wall of the process envelope		
Upper	15.6 ± 2.4	22.4 ± 3.7
Center	13.8 ± 1.6	25.6 ± 2.7
Lower	10.8 ± 1.6	23.0 ± 2.0
Coating thicknesses [nm] for the rear wall of the process envelope		
Upper	12.0 ± 1.4	24.2 ± 3.3
Center	23.2 ± 6.7	30.4 ± 2.9
Lower	19.6 ± 3.1	29.8 ± 3.5

homogeneously coated. It should be noted that local extremes of the microwave field have a direct effect on the film thickness distribution due to interference caused by the plasma configuration. Therefore, differences between the waveguides could be a cause for the fluctuations, but this cannot be conclusively proven. Furthermore, an inhomogeneous gas distribution can also contribute to an inhomogeneous layer thickness distribution. Earlier work on the reactor for large-area substrates at IKV demonstrated that the homogeneity of the layer thickness distribution is mainly dependent on the gas distribution [19]. There is potential for optimization here, as the holes in the process gas pipes can be adapted to the desired gas distribution.

A coating of the wafers arranged on the left by layer-forming particles from the plasma of the waveguide arranged in the center can play a subordinate role, as the measured layer thicknesses of the front wall are very low.

For the SiO_x layers, the clear demarcation of areas directly in front of and opposite the waveguides cannot be observed. The self-shielding of the plasma that is characteristic of the SiOCH layers is not present, so that all of the analyzed wafers have a layer thickness greater than 5 nm. Deposition rates vary between 0,3 nm/s and 0,9 nm/s. Consequently, the self-shielding of the plasma can be overcome by adjusting process conditions such as the pressure. When comparing the deposition rates for both layers to earlier studies of similar coatings, the SiO_x layers are in broad accordance with reported depositions rates of approx. 0.5 nm/s to 1 nm/s [20,21]. For the SiOCH layers however, deposition rates are reported much higher in the literature with values of 1.5 nm/s to 2 nm/s.

According to the parameters shown in Table 2, dyad layer systems consisting of an organic intermediate layer and an inorganic barrier layer were applied to the attached silicon wafers. The layer thickness distribution as a function of the position within the process envelope can be deducted from Table 5. At least a quadruple determination was carried out for all positions where a standard deviation is specified.

It is noticeable that thicker layers can be measured for the rear wall of the process envelope. This is potentially due to an asymmetrical process gas distribution within the process envelope. Looking at the process gas flow, the feed occurs on the right-hand side of the envelope. The first interaction with the microwave field occurs through the waveguide positioned at the center front. The resulting plasma could, for example, generate a partial pressure, which would orientate a larger proportion of the process gases towards the rear wall. This would result in a higher concentration of reactive particles and a correspondingly higher film deposition rate. As the system concept provides for the film to be transported through all horizontal positions, inhomogeneity can be compensated for more easily horizontally than vertically. To homogenize the vertical film thickness distribution, both the MW fields and the process gas flow should be homogenized.

Table 5
Layer thickness distribution for the dyad layer system according to Table 2.

Position	Left-hand side	Center
Coating thicknesses [nm] for the front wall of the process envelope		
Upper	10.0 ± 1.4	10.0 ± 2.8
Center	8.4 ± 2.3	9.6 ± 1.5
Lower	8.6 ± 3.7	15.0
Coating thicknesses [nm] for the rear wall of the process envelope		
Upper	20.6 ± 2.6	20.6 ± 2.9
Center	18.6 ± 1.7	19.6 ± 2.1
Lower	20.0 ± 1.9	22.8 ± 1.2

3.2. Investigation of parasitic coatings

To assess the functionality of the in-plasma principle, wafers were attached at various points within the process chamber. An overview of the wafers attached to the chamber wall is shown in Fig. 5.

In addition to the positions shown in Fig. 5, wafers were attached to the slits of the process envelope. Wafers were positioned at three heights directly on the process gas pipes according to the sampling positions. Three wafers were placed on the left rear side and three on the right front side of the process envelope. In the process chamber, the plasma process described above was carried out without the films in place to allow an estimate of the safe side. The coating time was 60 min. An overview of the coating thicknesses determined can be obtained from Table 6.

It can be observed that the highest layer thickness does not occur directly at the outlets of the process envelope, as expected, but at the chamber walls. Sample RR had the greatest layer thickness of all the samples analyzed. During sampling, it was observed that the coating on the chamber walls was most pronounced compared to the waveguide. Sample RR was located at the edge of the light cone of the center waveguide.

Sample FL was located in the light cone of the left waveguide and had the second thickest coating of the samples on the chamber walls. A clear differentiation of the measured values with regard to the main flow direction of the process gases escaping from the process envelope towards the TMP cannot be observed. The samples of the floor and ceiling panels have comparable layer thicknesses.

The samples, which were applied directly to the outlets of the process envelope, correspond to the observations from section 3.1. A clear coating can be observed on the wafers arranged on the left-hand side in contrast to the wafers arranged on the right-hand side. In addition, a clear increase in coating thickness can be observed over the height of the process envelope. A strong correlation with a dominant process gas flow towards the TMP can be assumed.

Consequently, the coating of the outlets appears to correlate more strongly with the process gas flow, while the coating of the chamber walls appears to be primarily related to the illumination with MW radiation. Due to the prevailing pressures and dimensions of the chamber, a molecularly dominated flow regime can be assumed outside the process envelope. The escaping reactive particles are probably accelerated towards the wall as a result of the interaction with the MW field. One measure to contain this effect could be to shield the cladding from the MW radiation. In addition to containing the parasitic coating, this would also lead to an increase in the energy density within the process envelope, which could have a positive effect on the layer deposition rate in the envelope.

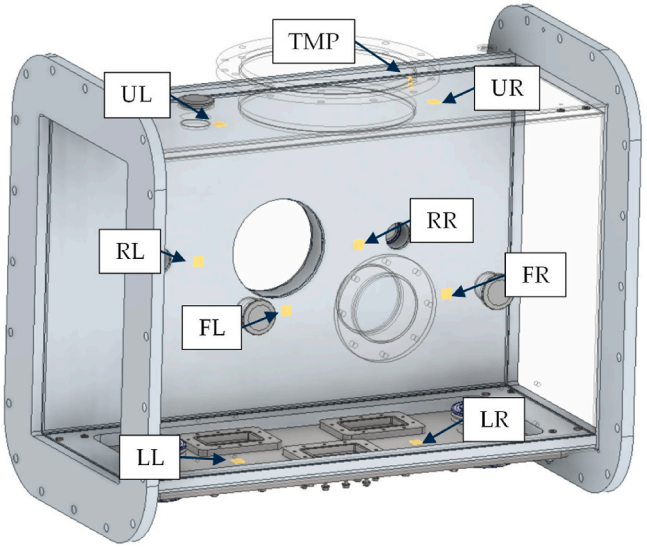

Fig. 5. Wafer positions for the determination of parasitic coatings.

Table 6
Determined coating thicknesses for the assessment of parasitic coatings.

Position	Left-hand side	Right-hand side
Coating thicknesses [nm]	Coating thickness [nm] on the chamber walls	
TMP	17.9 ± 2.5	
Upper wall	28.2 ± 3.3	<5
Front wall	69.4 ± 3.4	30.2 ± 3.5
Rear wall	<5	109.8 ± 8.6
Lower wall	23.0 ± 5.0	14.6 ± 1.7
Coating thicknesses [nm] at the rear left exit of the process envelope (see Fig. 2, upper right slit near process gas exhaust)		
Upper	70.8 ± 1.7	
Center	34.8 ± 1.2	
Lower	17.2 ± 2.8	
Coating thicknesses [nm] at the front right exit of the process envelope (see Fig. 2, lower left slit near process gas supply)		
Upper	<5	
Center	<5	
Lower	<5	

Looking at the most heavily coated position RR, a significant reduction in the film deposition rate compared to the inside of the process envelope can be observed. The film deposition rate inside the process envelope is approx. 0.6 nm/s, while it is approx. 0.03 nm/s for the HR position. The film deposition rate could therefore be reduced by a factor of 20 for the most heavily coated area. The measures described above should lead to an increase in this factor. For the outlet of the process envelope, the film deposition rate on the top left-hand side is approx. 0.02 nm/s and corresponds to a factor of 30. It can be assumed that this value is significantly reduced in the presence of a film in the gap due to the reduction in gap height. Nevertheless, constructive measures to reduce the conductance values of the outputs of the process envelope appear necessary, as the contactless insertion and removal of the film is necessary for the operation of the system.

3.3. Chemical composition

Based on the layer thickness distribution, a high spatial dependence of the layer deposition can be observed. In order to gain a better understanding of the chemical properties, location-dependent FT-IR analyses were carried out for the dyad coating system. Selected spectrograms can be seen in Figs. 6 and 7. The position relative to the waveguides can be observed as the most dominant influencing factor on the coating chemistry.

In Fig. 6, clear CH_3 bands can be observed for position FCU, which is located directly in front of the center waveguide. These bands are not pronounced for the two positions FLU and FLC, which are located opposite the left waveguide. In addition, FCC has a pronounced Si-O-Si network band in contrast to FLU and FLC. In contrast to FCU, FLU and FLC also have a pronounced Si-OH band. The Si-O-Si cage and Si-$(CH_3)_3$ bands are pronounced for all positions.

The spectrograms can be interpreted according to the layer thickness measurements of the individual SiOCH and SiO_x layers. Consequently, the bands specific to position FCU are due to the presence of the interlayer in the dyad system. Since the SiOCH layer is only deposited directly in front of the waveguides, the corresponding bands for the left side (FLU and FLC) are not detected.

In Fig. 7, an image exactly analogous to Fig. 6 can be observed, which corresponds to a symmetrical swapping of the center and left positions. The bands representative of the SiOCH layer are only detected for position RLU, which is located in front of the left waveguide. Despite the fact that the left region of the cladding is downstream of the center position, no significant differences are detected between RLU and FCU. Consequently, the position relative to the waveguide influences the

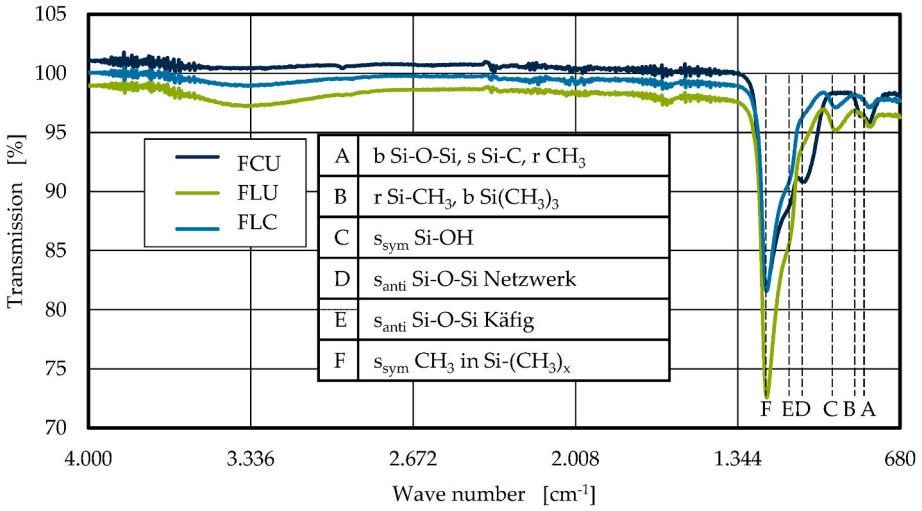

Fig. 6. FTIR spectrogram of selected positions on the front wall of the process envelope.

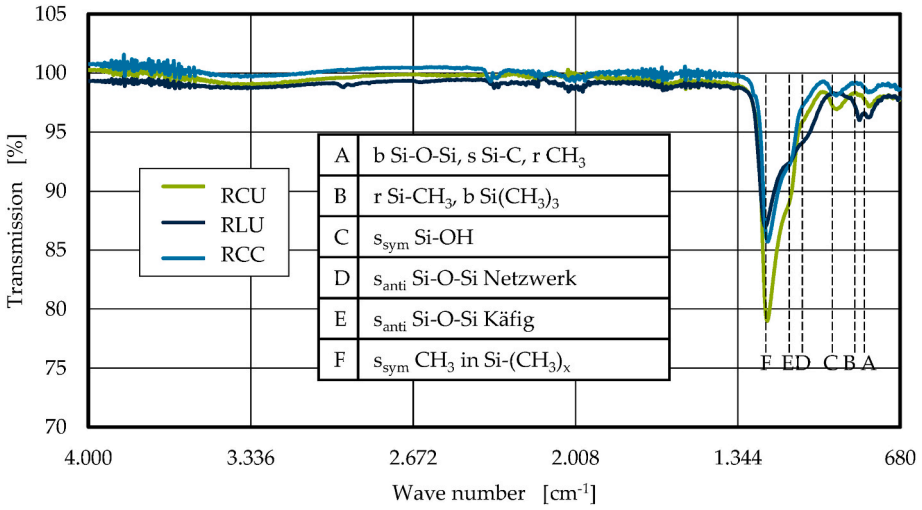

Fig. 7. FTIR spectrogram of selected positions on the rear wall of the process envelope.

layer chemistry significantly more than the position relative to the process gas inlet and outlet. The characteristic bands mentioned are very similar with regard to the vertical arrangement, so that the spectra shown are given as representative examples.

With regard to scaling the process, it can be assumed that layer deposition rates can be achieved by increasing the gas flow and adding additional waveguides without negatively influencing the layer chemistry.

3.4. Evaluation of the barrier effect

To assess the barrier effect against oxygen, film samples were taken at the positions defined above. The area of the samples subjected to OTR analysis corresponded to a diameter of 48 mm. The results are shown in Table 7. A triplicate determination was carried out for all positions where a standard deviation is given. A value of 132.5 ± 8.1 cm^3(STP)/day*m^2 was determined for the OTR of the uncoated film. The value is given in the data sheet for the same measurement conditions as 130 cm^3(STP)/day*m^2 [22].

It has been demonstrated that, in contrast to the layer thickness distribution of the dyad (see Table 5), the OTR values are predominantly dependent on the position relative to the waveguide. Significantly lower OTR values are observed for the front center and rear left positions,

Table 7
Spatially dependent OTR analysis of coated PET samples.

Position	Left-hand side		Center	
	OTR [cm^3(STP)/Tag*m^2]	BIF	OTR [cm^3(STP)/Tag*m^2]	BIF
Front wall of the process envelope				
Upper	19.2 ± 3.5	6.9	5.5 ± 0.1	24.2
Center	113.5 ± 13.4	1.2	9.3 ± 4.8	14.3
Lower	126.0 ± 7.2	1.1	6.3 ± 0.3	21.0
Rear wall of the process envelope				
Upper	4.5 ± 0.9	29.5	18.2 ± 2.0	7.3
Center	9.2 ± 4.7	14.4	119.0 ± 19.0	1.1
Lower	6.2 ± 0.4	21.4	122.0	1.1

which are directly in front of the waveguide, in comparison to the opposite positions. Despite the distribution of the dyad coating at all the positions considered, the barrier effect has been found to occur in the areas mentioned. Furthermore, an examination of the coating thickness distribution of the SiOCH and SiO_x layers reveals that the presence of the intermediate layer is a prerequisite for the manifestation of the barrier effect in the experiments presented. It has to be noted that the reactor has to be equipped with a second process chamber in order to apply two separate coatings inline. However, it has been shown that the

functionalization of the PET film used in this study was achieved by a single layer coating on a different reactor [21].

The homogeneity of the barrier effect is significantly higher when viewed vertically, with the lowest OTR values observed at the upper positions and the highest values observed in the center. As the microwaves are fed in over the entire surface without slots, the field densities can be higher at the ends of the waveguide opening. It must also be taken into account that the gas distribution has not yet been optimized. At the time of the experiments, the process gases are supplied and extracted via the base plate and by means of equidistant boreholes of the same diameter. Due to the resulting asymmetry, it can be assumed that there is potential to be exploited regarding the homogenization of the gas flow.

Ultimately, the process parameter space offers potential for homogenizing the deposition of the SiOCH layers. The plasma appears to exhibit a high degree of self-shielding in the SiOCH process step, which suppresses the coating of the surfaces opposite the waveguides. The MW field cannot penetrate the plasma due to the high plasma frequency, so that no sufficient particle density is achieved on the opposite wall. As the plasma frequency correlates with the electron density, a reduction in the energy density can be used as a strategy for homogenizing the layer deposition rate [8]. This in turn can be achieved by reducing the average power or by increasing the monomer flow. In terms of economic efficiency, a resulting reduction in the layer deposition rate is not an obstacle, as the SiOCH process step takes significantly less time than the SiO_x process step (Table 2).

The adaptation of the intermediate layer is essential for the transfer of the coating system to other substrates. Especially for non-polar and thermally sensitive substrates such as polyolefins, chemical bonds must be established without degrading the surface [23].

In addition to the achievable barrier properties, the time required to produce the coating system is also important for the economic efficiency of the reactor concept. As the highest barrier effect was observed for the left rear and center front positions, the barrier function was analyzed as a function of the coating time for the RLU position. An overview can be seen in Fig. 8. The coating time of 35 s corresponds to the initial parameters (Table 2).

The OTR decreases with increasing coating time and reaches a plateau at approx. 35 s. Based on the observed barrier effect, a closed coating can be assumed for all test points. With increasing coating thickness, only marginal improvements in the barrier effect are achieved, as existing defects cannot be closed. At higher layer thicknesses, the defect density can increase due to intrinsic stresses, so that the barrier effect decreases again [24]. Together with the requirement for a low layer thickness to improve the strain tolerance and the economic implications, the thinnest possible coating is desirable.

The coating deposition rate was determined to be approx. 0.62 nm/s based on the coating thicknesses for 25 and 30 s (16.5 nm and 20.6 nm). Assuming linear film growth after the formation of a closed film, a film thickness of approx. 9 nm can be assumed for 15 s. With regard to the vertical layer thickness distribution, the minimum layer thickness for the thinnest coated area must be fulfilled. Consequently, further homogenization of the coating thickness distribution is necessary for economical operation of the system. Nevertheless, the basic feasibility of barrier functionalization can be assessed as clearly positive.

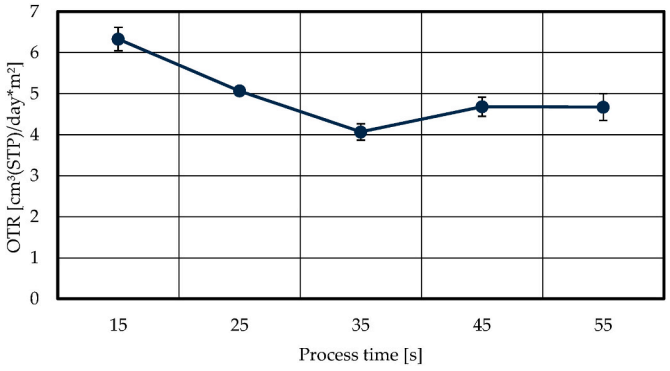

Fig. 8. OTR as a function of the coating time for position RLU.

4. Conclusion

The function of the process envelope as an equivalent to the hollow body was demonstrated, and the in-plasma principle was successfully transferred to the coating of films. To assess the containment of parasitic coatings, layer thickness measurements were carried out outside the process envelope, and it was demonstrated that the coating deposition rate is highest at one point on the chamber wall. For this location, the coating deposition rate was a factor of 20 lower than inside the process envelope.

Since the location with the highest deposition rate was in the illumination area of one of the waveguides, additional shielding of the process envelope can minimize the coating of the chamber walls.

The second most heavily coated area was located directly at the top of the left-hand exit of the process envelope, where reactive species escape through the film gap. Here, the film deposition rate was reduced by a factor of 30. It should be noted that the tests were carried out as a safe estimate without the presence of the film in the gap. Although the film minimizes gas exchange and thus the escape of reactive species, particular attention must be paid to the clogging of the slits. The contactless insertion and removal of the film is a necessary prerequisite for the function of the system and must be examined more closely in order to estimate maintenance intervals for replacing or cleaning the process envelope.

When evaluating the homogeneity of the deposited layers within the process envelope, very different behavior can be observed for the deposition of the SiOCH and SiO_x layers. While the SiO_x layer can be detected within the process envelope in the entire area illuminated with MW radiation, the SiOCH layer can only be detected directly on the waveguides. One possible reason for this is self-shielding of the plasma due to a higher electron density compared to the SiO_x plasma. Since HMDSO molecules fragment faster than oxygen molecules a heightened fragmentation rate and electron density is conceivable. This in return would lead to a shortened Debye radius and a cut off of incoming microwave radiation [9,25].

Over the length of the waveguide, inhomogeneous vertical layer thickness distribution could be detected for both process steps. The reason for this could be the gas distribution within the process envelope. Improving this is highly desirable, as horizontal inhomogeneities will be compensated for in the future by the movement of the film web. Vertical inhomogeneities, on the other hand, would remain. Since the process gas pipes are fed from below (Figs. 3 and 4), a pressure gradient develops within the pipes, which decreases from bottom to top. To counteract this, the bore radii could be increased towards the top or the spacing or number of bores could be adjusted. One approach to estimating the resulting gas distribution is to use neutral gas simulations.

In summary, it can be stated that the first gas barrier coatings were successfully deposited in the novel reactor. This represents a decisive milestone in the implementation of the reactor concept, as the compatibility of the leakage-prone airlock systems with the PECVD process was previously unclear. Furthermore, a significantly lower degree of coating deposition on the chamber walls (parasitic coatings) was observed in comparison to the inside of the process envelope.

The barrier improvement factors achieved were in the range of 20–30 for waveguides. Furthermore, parameter sets for SiOCH and SiOx layer systems were found. The use of SiOCH intermediate layers contributed to significant improvements in barrier performance in the study. A procedure for homogenizing the layer thickness distribution was demonstrated, as its implementation is considered particularly important for the effectiveness of the reactor concept.

CRediT authorship contribution statement

Philipp Alizadeh: Writing – original draft, Validation, Data curation, Conceptualization. **Rainer Dahlmann:** Writing – review & editing, Supervision, Project administration, Funding acquisition.

Data availability statement

The data that support the findings of this study are available from the corresponding author upon reasonable request.

Declaration of competing interest

The authors declare no financial or commercial conflict of interest.

Acknowledgements

The work shown in this article received support of the German Research Foundation (DFG) within the framework of the Trans Regional Collaborative Research Centre TRR 87/1 (SFB-TR 87) "Pulsed High Power Plasmas for the Synthesis of Nanostructural Functional Layers" transfer project T06 "Low-maintenance continuous Air2Air PECVD film coating via an In-Plasma concept (In-Plasma-Air2Air)". We would like to thank the DFG and our project partners from the industry.

References

[1] Eurostat, Municipal Waste by Waste Management Operations, 2022.
[2] Directive 2008/98/EC of the European parliament and of the council of 19 November 2008 on waste and repealing certain directives *[Online]*. Available: http://data.europa.eu/eli/dir/2008/98/oj, 2024. (Accessed 4 February 2025).
[3] KHS GmbH, InnoPET plasmax barrier technology: internal coating of your PET bottles with high-quality SiOx. [Online]. Available: https://www.khs.com/en/products/machines-equipment/detail/innopet-plasmax-barrier-technology (accessed: February. 4 2025).
[4] P. Plein, Method of Coating Hollow Bodies, Apr 7, 1988. DE3632748 (A1).
[5] J.M. Rius, Device for Treating Containers with a Low Pressure Plasma and an Associated Vacuum Circuit of Economic and Reliable Design, Apr 27, 2001. FR2799994 (A1).
[6] J. Laurent, Method and Apparatus for Treating the Inside Surface of Plastic Bottles in a Plasma Enhanced Process, Jul 19, 2000. EP1019944 (A1).
[7] M. Jaritz, Coating Technology for Plastic Containers, Oct 30, 2024. EP4453274 (A1).
[8] F. Paschen, Ueber die zum Funkenübergang in Luft, Wasserstoff und Kohlensäure bei verschiedenen Drucken erforderliche Potentialdifferenz, Ann. Phys. 273 (5) (1889) 69–96, https://doi.org/10.1002/andp.18892730505.
[9] A.A. Fridman, Plasma Chemistry, Cambridge Univ. Press, Cambridge, New York, 2008.
[10] C. Rovera, M. Ghaani, S. Farris, Nano-inspired oxygen barrier coatings for food packaging applications: an overview, Trends Food Sci. Technol. 97 (2020) 210–220, https://doi.org/10.1016/j.tifs.2020.01.024.
[11] K. Müller, et al., Review on the processing and properties of polymer nanocomposites and nanocoatings and their applications in the packaging, automotive and solar energy fields, Nanomaterials 7 (4) (2017), https://doi.org/10.3390/nano7040074.
[12] C. Bishop, Vacuum Deposition onto Webs, Films, and Foils, William Andrew/Elsevier, Amsterdam, Boston, 2011 [Online]. Available: https://www.sciencedirect.com/science/book/9780323296441.
[13] C.R. Bening, J.T. Pruess, N.U. Blum, Towards a circular plastics economy: interacting barriers and contested solutions for flexible packaging recycling, J. Clean. Prod. 302 (2021) 126966, https://doi.org/10.1016/j.jclepro.2021.126966.
[14] Allied Market Research, *Packaging coatings market: global opportunity analysis and industry forecast, 2021-2030*. Size, share, competitive landscape and trend analysis report, by application), type, end-user, substrate. [Online]. Available: https://www.alliedmarketresearch.com/packaging-coatings-market (accessed: January. 8 2025).
[15] P. Alizadeh, R. Dahlmann, Vacuum technical investigation of a novel reactor for the continuous coating of flexible web material, Vacuum 240 (2025) 114579, https://doi.org/10.1016/j.vacuum.2025.114579.
[16] A. Grill, D.A. Neumayer, Structure of low dielectric constant to extreme low dielectric constant SiCOH films: fourier transform infrared spectroscopy characterization, J. Appl. Phys. 94 (10) (2003) 6697–6707, https://doi.org/10.1063/1.1618358.
[17] J. Trieschmann, D. Hegemann, Plasma polymerization at different positions in an asymmetric ethylene discharge, J. Phys. D Appl. Phys. 44 (47) (2011) 475201, https://doi.org/10.1088/0022-3727/44/47/475201.
[18] R. Snyders, D. Hegemann, D. Thiry, O. Zabeida, J. Klemberg-Sapieha, L. Martinu, Foundations of plasma enhanced chemical vapor deposition of functional coatings, Plasma Sources Sci. Technol. 32 (7) (2023) 74001, https://doi.org/10.1088/1361-6595/acdabc.
[19] D. Kirchheim, et al., Improved homogeneity of plasma and coating properties using a lance matrix gas distribution in MW-PECVD, J. Coating Technol. Res. 16 (2) (2019) 573–583, https://doi.org/10.1007/s11998-018-0138-4.
[20] P. Alizadeh, J. Franke, R. Dahlmann, Stretch-tolerant PECVD gas barrier coatings for sustainable flexible packaging, Plasma Process. Polym. (2024), https://doi.org/10.1002/ppap.202400018.
[21] M. Jaritz, P. Alizadeh, S. Wilski, L. Kleines, R. Dahlmann, Comparison of HMDSO and HMDSN as precursors for high-barrier plasma-polymerized multilayer coating systems on polyethylene terephthalate films, Plasma Process. Polym. (2021) 1–18, https://doi.org/10.1002/ppap.202100018.
[22] FlexFilms, *FLEXPET™ F-MTG*, *Technical data sheet*. Biaxially oriented polyester film [Online]. Available: https://www.flexfilm.com/pdf/Products/BOPET/F-MTG.pdf.
[23] P. Alizadeh, K. Oberle, R. Dahlmann, Process transfer of PECVD gas barrier coatings between PE-HD and PP hollow bodies, in: Proceedings of the 39th International Conference of the Polymer Processing Society (PPS-39), 2024, pp. 188–196, https://doi.org/10.51573/Andes.PPS39.GS.NN.2.
[24] M. Jaritz, et al., Comparative study of the residual stress development in HMDSN-based organosilicon and silicon oxide coatings, J. Phys. D Appl. Phys. 53 (34) (2020) 345203, https://doi.org/10.1088/1361-6463/ab8ceb.
[25] D. Hegemann, Plasma polymer deposition and coatings on polymers, in: Comprehensive Materials Processing, Elsevier, 2014, pp. 201–228.